A&A 374, 250–258 (2001)
DOI: 10.1051/0004-6361:20010729

Astronomy & Astrophysics

Pre-main sequence dynamos and relic magnetic fields of solar-type stars

L. L. Kitchatinov[1], M. Jardine[2], and A. Collier Cameron[2]

[1] Institute for Solar-Terrestrial Physics, PO Box 4026, Irkutsk 664033, Russia
[2] School of Physics and Astronomy, University of St Andrews, St Andrews, Fife KY16 9SS, Scotland
e-mail: mmj@st-andrews.ac.uk; acc4@st-andrews.ac.uk

Received 10 November 2000 / Accepted 19 May 2001

Abstract. We argue that contemporary magnetic fields in the radiative cores of solar-type stars are relics of hydromagnetic dynamos operating over the pre-main sequence epoch when the core formed. Simulations of differential rotation and dynamos of a 1 $M_\odot$ star are performed for a sequence of evolutionary stages of the core-growth epoch. A big difference in the dynamo-generated field between the initial and final stages of the core formation is predicted. An axisymmetric and cyclic field similar to the present day Sun is excited in a star with a mature radiative zone. An infant Sun with its core just starting to grow generates a nonaxisymmetric global field which is steady in a rotating frame. A qualitative explanation for the nonaxisymmetry is suggested. A model for the field capturing by the growing core is designed. The internal field is most efficiently captured over the initial phase when the core grows most rapidly. A nonaxisymmetric global relic field with an amplitude somewhat below 1 G is predicted for a main-sequence star of solar mass. An interpretation of the active longitude phenomenon as observed on the Sun and stars in terms of the nonaxisymmetric relic field is suggested.

Key words. stars: magnetic fields – stars: rotation – stars: interiors – stars: evolution – Sun: magnetic fields – MHD

1. Introduction

It is generally accepted that solar-type stars possess magnetic fields in their radiative cores. The internal fields are important for the rotational coupling between the core and convection zone (Spruit 1987; Charbonneau & McGregor 1992, 1993) that is evident from helioseismology (Shou et al. 1998). Also the observed alteration of high and low activity cycles on the Sun is readily explained in terms of a weak internal magnetic field (Pudovkin & Benevolenskaya 1984).

The field is usually assumed to be a relic of the pre-main sequence epoch. The microscopic magnetic diffusivity of the core $\sim 10^3$ cm^2 s^{-1} is low enough for the field to survive against ohmic decay over evolutionary times. The question of how the relic field is attained by the core is much less clear, however. A considerable flux can be captured from a protostellar cloud by the forming star (Mestel 1965). Later on, the star evolves through a fully-convective stage. The duration of this stage, $\gtrsim$1 Myr, is about 10^4 times longer than the characteristic time of turbulent diffusion. It is quite problematic for a global primordial field to survive the Hayashi-phase.

It could do so only if turbulent diffusion were not active for some reason. The spatial separation of magnetic and velocity fields on small scales (Tayler 1987) and suppression of the turbulent fragmentation of scales in a 2D flow (Cattaneo & Vainshtein 1991) were suggested as possible reasons. The possibilities seem to be limited to very special cases of hydromagnetic turbulence (Nordlund et al. 1994).

Rotating convective stars can drive hydromagnetic dynamos. The observed magnetic activity of T Tauri stars (e.g., Gilliland 1986; Basri et al. 1992) supports this expectation. The dynamo-generated field can then be incorporated into the growing radiative core (Schussler 1975; Parker 1981; Dudorov et al. 1989). In this scenario, the global geometry and amplitude of the "relic" field are mainly controlled by the dynamo operating in the retreating convection zone.

This paper describes simulations of the convection zone dynamo and the internal field capture by a growing

Send offprint requests to: L. L. Kitchatinov,
e-mail: kit@iszf.irk.ru

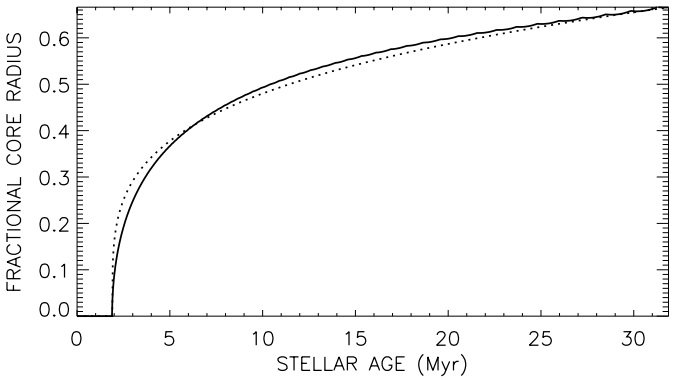

Fig. 1. Fractional radius, x_c, of the radiative core of the 1 $M_\odot$ star as a function of stellar age. The dotted line shows the power-law approximation, $x_c \sim (t - t_0)^{1/4}$.

radiative core for a solar mass star. We first model the evolution of the stellar structure over the core growth epoch. Then, the differential rotation and dynamo are simulated for several evolutionary stages. A nonaxisymmetric global field is predicted to be generated over the initial (most rapid) growth of the core. The field is steady in a rotating reference frame. The frame does not, however, co-rotate with the fluid. In the co-rotating frame, the nonaxisymmetric field pattern migrates over longitudes completing one revolution in (roughly) a diffusion time. The migration reduces the efficiency of the field capture, so that a kilogauss field in the convection zone decreases to about one Gauss in the internal field after being incorporated into a fully-grown core. This small field is sufficient to couple the core rotation to the convection zone. It also can be the reason for the axial asymmetry observed in magnetic activity of the Sun and stars.

The next Section describes the design of our models. Section 3 presents the results and discusses their implications.

2. Simulations

2.1. Stellar evolution

The dynamo simulations require a specification of the stellar structure. The evolution of the star was computed using Eggleton's (1971, 1972) code, which applies the equation of state of Eggleton (1973). For temperatures below 10^4 K where molecular opacities are important, the opacities are specified after Rogers & Iglesias (1992) and Weiss et al. (1990). The computations were made for a star of one solar mass, with a typical Population I composition $X = 0.70$ and $Z = 0.02$. The starting point for the model was a fully-convective protostar near the top of its Hayashi track, with radius 6 $R_\odot$. The star was evolved to a slightly pre-main sequence age of 32 Myr.

Figure 1 shows the ratio, $x_c = r_c/R$, of the core radius, r_c, to the radius of the star as a function of stellar age. At the end of the run, the core radius, $x_c = 0.67$, is close to the present-day solar value.

Table 1. Structure parameters for the pre-main sequence Sun.

Age, Myr	x_c	$L/L_\odot$	$R/R_\odot$	ρ_e, g cm^{-3}	T_e, K
1.92	0.05	1.14	2.01	6.40×10^{-3}	1.25×10^5
2.39	0.18	0.97	1.87	7.42×10^{-3}	1.31×10^5
4.32	0.34	0.63	1.65	1.13×10^{-2}	1.53×10^5
10.4	0.50	0.38	1.23	2.20×10^{-2}	2.19×10^5
31.9	0.67	0.63	1.05	1.32×10^{-2}	2.54×10^5

2.2. Differential rotation

Our differential rotation model is almost identical to that of Kitchatinov & Rüdiger (1999) (the only difference is discussed shortly below). A detailed description of the model can be found in that paper. We avoid reproducing it here.

The model defines the distributions of angular velocity, meridional flow and entropy within a convection zone provided that input stellar parameters are given. These include the stellar mass (M), total luminosity (L), radius (R), rotation period ($P_{\rm rot}$), fractional radius of the convection zone inner boundary (x_c), density (ρ_e), and temperature (T_e) at the external radius, $x_e = r_e/R$, of the simulation domain slightly below the stellar surface, and the mixing-length parameter, $\alpha_{\rm MLT} = \ell/H_p$, of the ratio of the mixing length to the pressure scale height. We applied quite a standard value $\alpha_{\rm MLT} = 1.7$ and put $x_e = 0.95$ in all simulations. The other parameters except for the rotation period are defined by the stellar evolution model. Table 1 lists the input parameters for the five stellar ages for which the differential rotation and dynamo simulations were performed. Note that the five states are approximately equally spaced in core radius.

A new feature of the problem concerned is that energy release within the convection zone cannot be neglected. Accordingly, we have to modify the heat transport equation (Eq. (18) of Kitchatinov & Rüdiger 1999) by including the source term into its right side:

$$\mathrm{div}\left(\boldsymbol{F}^{\rm conv} + \boldsymbol{F}^{\rm rad}\right) + \rho T \boldsymbol{u}\cdot\boldsymbol{\nabla} S = \frac{1}{4\pi r^2}\frac{\partial \mathcal{L}}{\partial r}\,, \qquad (1)$$

where $\mathcal{L}$ is the local luminosity, S is entropy, $\boldsymbol{F}^{\rm conv}$ and $\boldsymbol{F}^{\rm rad}$ are the convective and radiative heat fluxes respectively.

Figure 2 shows an example of the computed differential rotation for the age 1.92 Myr. The rotation period $P_{\rm rot} = 5$ day for this case. The surface differential rotation is only $\simeq$0.3%. The small rotational inhomogeneity is, nevertheless, significant for the dynamo. It is also somewhat larger than predicted by Küker & Rüdiger (1997). The difference is due to the account taken of thermodynamics in our model. The sharp changes in the angular velocity near the top and bottom show the boundary layers (Durney 1989; Kitchatinov & Rüdiger 1999).

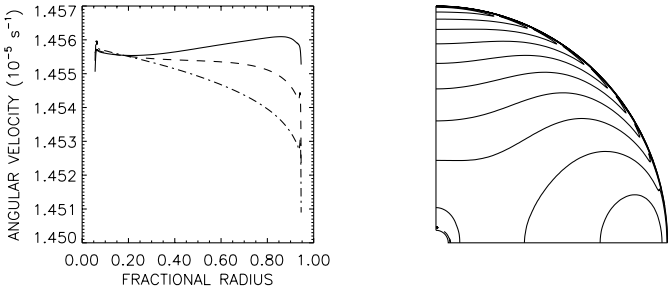

Fig. 2. Rotation law for the 1.92 Myr aged 1 $M_\odot$ star predicted by our differential rotation model. Left: depth profiles of the angular velocity for the equator (full line), 45°-latitude (dashed), and pole (dashed-dotted). Right: angular velocity isolines. $P_{\rm rot} = 5$ day.

The meridional flow is strongly limited to these layers. The flow amplitude is about 10 m s^{-1} at the boundaries but falls well below 1 m s^{-1} within a short distance. The slow circulation is neglected in the dynamo simulations.

The differential rotation model also supplies the radial profiles of the eddy diffusivity and some other parameters required for dynamo simulations (cf. Fig. 3).

2.3. Dynamo model

We simulate dynamo action in a stellar convection zone by solving the mean-field induction equation,

$$\partial \boldsymbol{B}/\partial t \;=\; {\rm rot}\,(\boldsymbol{V}\times\boldsymbol{B} \;+\; \boldsymbol{\mathcal{E}})\,, \tag{2}$$

in a spherical layer. The large-scale velocity field, $\boldsymbol{V}$, stands for a non-uniform rotation,

$$\boldsymbol{V} = \boldsymbol{e}_\phi r\;\sin\theta\;\Omega(r,\theta), \tag{3}$$

where $\boldsymbol{e}_\phi$ is the azimuthal unit vector and r, θ and ϕ are the usual spherical coordinates.

The mean electromotive force, $\boldsymbol{\mathcal{E}}$, of the induction Eq. (2) is produced by the correlated fluctuations of magnetic, $\boldsymbol{B'}$, and velocity, $\boldsymbol{u'}$, fields (cf. Krause & Rädler 1980),

$$\boldsymbol{\mathcal{E}} \;=\; \overline{\boldsymbol{u'}\times\boldsymbol{B'}} \;=\; \boldsymbol{\mathcal{E}}_{\rm diff} + \;\boldsymbol{\mathcal{E}}_{\rm gen}. \tag{4}$$

This equation distinguishes the contributions made by turbulent diffusion and by magnetic field generation due to the α-effect of cyclonic convection (Parker 1979).

The diffusive part allows for rotationally-induced anisotropy and quenching (Kitchatinov et al. 1994),

$$\boldsymbol{\mathcal{E}}_{\rm diff} = -\eta\;{\rm rot}\boldsymbol{B} \;-\; \eta_\parallel \boldsymbol{e}\times((\boldsymbol{e}\cdot\nabla)\boldsymbol{B})\,, \tag{5}$$

where $\boldsymbol{e} = \boldsymbol{\Omega}/\Omega$ is the unit vector along the rotation axis and $\eta_\parallel$ is the diffusivity excess along this axis compared to the transverse direction. The rotational effects on the diffusivities,

$$\eta \;=\; \eta_{\rm T}\phi(\Omega^*),\quad \eta_\parallel \;=\; \eta_{\rm T}\phi_\parallel(\Omega^*), \tag{6}$$

are involved via the dimensionless quenching functions, $\phi(\Omega^*)$ and $\phi_\parallel(\Omega^*)$ (Kitchatinov et al. 1994),

$$\begin{aligned}
\phi(\Omega^*) \;&=\; \frac{3}{4\Omega^{*2}}\left(1 \;+\; \frac{\Omega^{*2}-1}{\Omega^*}{\rm tan}^{-1}\,(\Omega^*)\right),\\
\phi_\parallel(\Omega^*) \;&=\; \frac{3}{4\Omega^{*2}}\left(-3 \;+\; \frac{\Omega^{*2}+3}{\Omega^*}{\rm tan}^{-1}\,(\Omega^*)\right),
\end{aligned} \tag{7}$$

of the local Coriolis number,

$$\Omega^* = \;2\tau\Omega, \tag{8}$$

where τ is the convective turnover time.

The efficiency of a shear flow in generating a magnetic field can be estimated by a dimensionless product of the time of the field diffusion, l^2/η, over a spatial scale, l, of the shear region with the field winding frequency, $R\Delta\Omega/l$. The estimations show that the boundary layers of Fig. 2 are of minor importance for the dynamo. We exclude the very thin boundary layers from the computational domain to avoid problems with numerical resolution.

The generation part, $\boldsymbol{\mathcal{E}}_{\rm gen}$, of the mean electromotive force (4) is expressed in terms of the $\boldsymbol{\alpha}$-tensor,

$$\boldsymbol{\mathcal{E}}_{\rm gen} = \;\boldsymbol{\alpha}\circ\boldsymbol{B}. \tag{9}$$

A mixing-length representation for this tensor for a density-stratified rotating fluid (Rüdiger & Kitchatinov 1993),

$$\alpha_{ij} = -\,(\boldsymbol{e}\cdot\boldsymbol{G})\,(\delta_{ij}a_1 + \;e_ie_ja_4) \;-(e_iG_j + e_jG_i)\,a_2, \tag{10}$$

is applied. In this equation, $\boldsymbol{G} = \nabla{\rm ln}(\rho)$ is the density stratification vector and a_n-coefficients,

$$a_n = \;\eta_{\rm T}\mathcal{A}_n(\Omega^*), \tag{11}$$

are expressed in terms of the eddy diffusivity and further quenching functions, $\mathcal{A}_n$ (Rüdiger & Kitchatinov 1993),

$$\begin{aligned}
\mathcal{A}_1 \;&=\; \frac{3}{2\Omega^{*3}}\left(\Omega^{*2}+6-\frac{6+3\Omega^{*2}-\Omega^{*4}}{\Omega^*}{\rm tan}^{-1}\,(\Omega^*)\right),\\
\mathcal{A}_4 \;&=\; \frac{3}{2\Omega^{*3}}\left(\Omega^{*2}-30-\frac{2\Omega^{*4}}{1+\Omega^{*2}}\right.\\
&\qquad\left.+\frac{30+9\Omega^{*2}-\Omega^{*4}}{\Omega^*}{\rm tan}^{-1}\,(\Omega^*)\right),\\
\mathcal{A}_2 \;&=\; -4\phi_\parallel\,(\Omega^*)\,/\Omega^*\,,
\end{aligned} \tag{12}$$

where the function $\phi_\parallel$ is defined by Eq. (7).

The notation, $\eta_{\rm T}$, of the above equations stands for the magnetic eddy diffusivity which would exist under actual sources of turbulent convection (actual superadiabaticity) if rotation were absent. Rotational effects are involved through the quenching functions (6). Accordingly, the mixing length expression for non-rotating fluids,

$$\eta_{\rm T} = -\frac{\tau\ell^2 g}{12c_{\rm p}}\frac{\partial S}{\partial r}, \tag{13}$$

can be applied, where the entropy gradient is supplied by the differential rotation model which also yields the profiles for the Coriolis number and density gradient. Figure 3

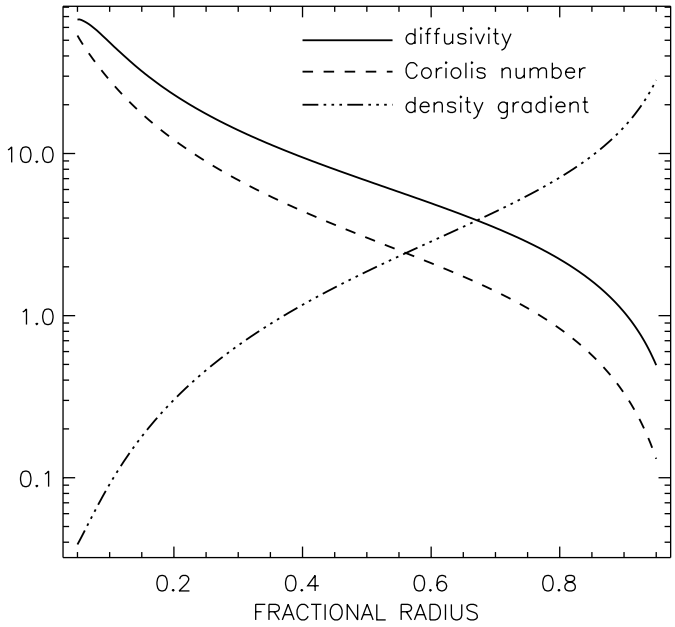

Fig. 3. Eddy diffusivity, $\eta_{\rm T}$ (13), in units of 10^{14} cm^2 s^{-1}, Coriolis number (8) divided by one hundred, $\Omega^*/100$, and the density startification parameter, $-rG = -\partial\ln(\rho)/\partial\ln(r)$, as functions of fractional radius. The profiles are supplied by the differential rotation model of 1.92 Myr old star with $P_{\rm rot} = 5$ day.

shows the profiles for 1.92 Myr aged star provided by the differential rotation model of Fig. 2 (note that constant scaling factors are introduced to plot the parameters dispersed by several orders of magnitude on the same figure).

This paper concerns kinematic dynamos that neglect any back reaction of the generated fields on the fluid motion. In this case, the complete system of dynamo equations splits into independent subsystems governing the field constituents of different types of equatorial and axial symmetries. In other words, the field components of different symmetry types behave independently. We shall use the traditional (cf., e.g., Krause & Rädler 1980) notations, Sm and Am, for the symmetry types, where the capital A or S signify the antisymmetric or symmetric field, respectively, relative to the mirror-reflection about the equatorial plane and "m" is the azimuthal wave-number. E.g., S0 means an equatorially and axially symmetric field while A1 signifies an antisymmetric field about the equator which is also nonaxisymmetric with two changes of the field sign over a longitudinal circle.

Normalized $\alpha^2\Omega$-dynamo equations possess two governing parameters measuring the efficiency of global and small-scale motions in generating magnetic fields:

$$C_\Omega = \frac{\Delta\Omega R^2}{\eta}, \quad C_\alpha = \frac{\alpha_{\phi\phi} R}{\eta}, \tag{14}$$

where $\Delta\Omega$ is the equator-to-pole difference in the surface angular velocity, and the values of the $\alpha_{\phi\phi}$-component of the α-tensor and the diffusivity, η, are taken at the midpoint, $x = (x_{\rm c} + x_{\rm e})/2$, of the convection zone.

The C_Ω-value is fixed by the differential rotation simulation. C_α (14) is therefore the only free parameter of our dynamo model. Remember that the dynamo-effect takes place only if C_α exceeds some threshold value. The value depends on the global symmetry of the field. We shall compute the threshold C_α values for different types of the symmetry. The motivation comes from the notion that the magnetic field back reaction on the small-scale motions reduces the α-effect, so that the effective C_α is decreased to the threshold value. Then, the nonlinear solution is normally close to the symmetry type of the kinematic dynamo-mode that has the smallest C_α required for its excitation (Krause & Meinel 1988; Brandenburg et al. 1989), though exceptions from the rule can be found in the literature (Rädler et al. 1990; Moss et al. 1991, 1992). In this sense, the kinematic mode with the smallest critical C_α represents the "preferentially excited" magnetic field.

The superconductor boundary condition was imposed at the bottom. The condition requires the tangential component of the mean electromotive force (4) be zero on the boundary,

$$\boldsymbol{n} \times \boldsymbol{\mathcal{E}} \;=\; 0 \quad \text{at } r = r_{\rm c}, \tag{15}$$

where $\boldsymbol{n}$ is the unit vector normal to the boundary. The strong magnetic fields of rapid rotators are expected to erupt almost freely through the top boundary. The open-type vacuum boundary condition was applied on the top. The magnetic field representation for spherical geometry which distinguishes its toroidal, $\boldsymbol{B}_{\rm t}$, and poloidal, $\boldsymbol{B}_{\rm p}$, components (Chandrasekhar 1961),

$$\boldsymbol{B} = \boldsymbol{B}_{\rm t} + \boldsymbol{B}_{\rm p} = -\boldsymbol{r} \times \nabla T \;-\; \mathrm{rot}\left(\frac{\boldsymbol{r}}{r} \times \nabla P\right), \tag{16}$$

helps to specify the condition explicitly. The vacuum condition (cf. Krause & Rädler 1980) requires the toroidal field to vanish (otherwise there are finite currents across the boundary) and the poloidal field to smoothly fit the potential external field:

$$T = 0, \quad \frac{\partial a_\ell^m}{\partial r} = -\frac{\ell}{r} a_\ell^m \quad \text{at} \quad r = r_{\rm e}, \tag{17}$$

where $a_\ell^m(r)$ are the amplitudes of the poloidal field expansion in terms of the spherical functions,

$$P \;=\; \sum_{\ell=1}^{L} \sum_{m=0}^{\ell} a_\ell^m(r) P_\ell^m(\cos\theta) \mathrm{e}^{\mathrm{i}m\phi}, \tag{18}$$

P_ℓ^m are the adjoint Legendre polynomials. The expansion (18) is forced by the nonlocal nature of the vacuum condition.

The eigenvalue problem for the dynamo equations was solved numerically by the inverse iteration method.

3. Results and discussion

3.1. Infant Sun dynamo

Dynamo simulations for the youngest of our chosen stars show a clear preference for a *nonaxisymmetric* magnetic field.

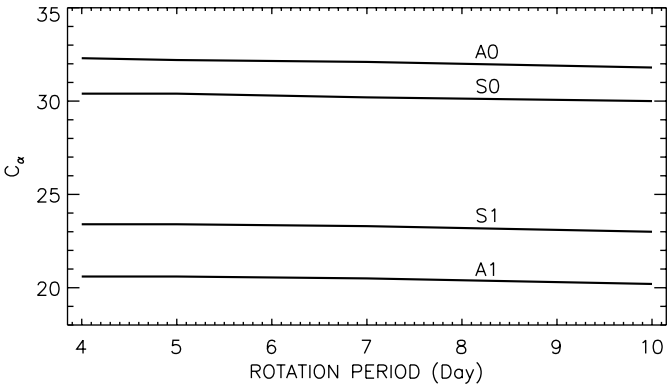

Fig. 4. Critical C_α (14) for the excitation of magnetic fields of different axial and equatorial symmetries as functions of the rotation period. The capital S and A in the notations Sm and Am signify equatorially-symmetric and antisymmetric fields, respectively, while "m" is the azimuthal wave-number.

The star at the age of 1.92 Myr is almost fully convective with the fractional core radius slightly below 0.05. Characteristic equatorial rotation rates of very young T-Tauri stars are about 20 $\mathrm{km\,s^{-1}}$ (Hartmann & Noyes 1987). Simulations were performed for several rates between 10 and 25 $\mathrm{km\,s^{-1}}$ with very similar results for all cases. Figure 4 shows the threshold values of the C_α-parameter (14) for excitation of magnetic fields of different symmetry types as functions of the rotation period. For azimuthal wave numbers larger than one the critical values of C_α are much higher than that shown on this figure.

As we shall see below, the internal field is captured most efficiently at the earliest stages of the (most rapid) core growth. The finding of nonaxisymmetry for that epoch is a significant result. There are two basic reasons for the nonaxisymmetry: (i) small differential rotation, and (ii) anisotropy of the alpha-effect (Rüdiger & Elstner 1994; Moss & Brandenburg 1996).

Rädler (1975) noticed that a strong differential rotation inhibits deviations from axisymmetry by converting an azimuthal inhomogeneity of a magnetic field into a small-scale radial and/or latitudinal inhomogeneties, thus amplifying the diffusive decay. The differential rotation of Fig. 2 is quite small. The C_Ω parameter (14) estimated with the surface differential rotation is $C_\Omega = 240$ and the differential rotation in deeper layers is smaller still (for comparison, $C_\Omega \sim 10^3$ for the present-day Sun). Our model may, however, underestimate the angular velocity inhomogeneity in the rapid rotators. The underestimation is by a factor of about two in the case of the extremely rapid rotation of AB Doradus (Donati & Cameron 1997; Kitchatinov & Rüdiger 1999). We repeated some runs with the differential rotation amplified by a factor of 3 to find a still clear preference for the nonaxisymmetric fields.

The small differential rotation opens a possibility for the nonaxisymmetric fields to survive while the special structure of the α-effect for the rapid rotation case ensures their preference. Coriolis numbers (8) for the star concerned are large, $\Omega^* \gtrsim 100$, and the α-tensor (10) for this case,

$$\alpha_{ij} = \frac{3}{4}\pi\eta_{\mathrm{T}} G\,(\delta_{ij} - e_i e_j)\cos\theta \qquad (19)$$

is anisotropic. The anisotropy accounted for by the $e_i e_j$-term in the brackets means in particular that there is no α-effect for magnetic fields parallel to the rotation axis. Such an anisotropy is readily explained by the anisotropy of turbulent motions. The known property of turbulence is that it becomes almost two-dimensional under the rapid rotation condition with the flow almost uniform along the rotation axis. If a magnetic field is parallel to this axis, two-dimensional turbulence can only interchange but not deform the field-lines. The α-effect can only be produced via field-line deformation (Parker 1955). Accordingly, the generatory part (9) of the mean electromotive force vanishes for a magnetic field parallel to the rotation axis. The α-effect is reestablished, however, for the fields inclined to the axis of rotation and is largest for an orientation normal to the axis. It may also be noted that Eq. (19) gives the largest values on the rotation axis due to the $\cos\theta$-dependence on latitude.

Summing-up, the α-effect is most powerful on the axis of rotation with the magnetic field normal to the axis. Only the nonaxisymmetric magnetic fields with $m = 1$ possess on the rotation axis a finite component normal to the axis. In other words, only the nonaxisymmetric fields can "use" the α-effect in the region where the effect is most powerful. This is, perhaps, the reason why nonaxisymmetry is preferred under rapid, almost uniform rotation.

To visualize the 3D fields, we use the representation (16) for the magnetic field which distinguishes its toroidal and poloidal constituents. The toroidal field-lines lie on concentric spherical surfaces. The poloidal fields are supported by toroidal currents. The marginal A1 and S1 modes for $P_{\mathrm{rot}} = 5$ day are illustrated by Figs. 5 and 6.

3.2. The age dependence: From nonxisymmetry to axisymmetry

Figure 7 shows the dependence on stellar age of the threshold dynamo-numbers. There is a change in the symmetry type of the preferred dynamo mode between the initial and final stages of the core growth. Axisymmetric fields oscillating with a period $P_{\mathrm{cyc}} \sim 10$ yrs are predicted for the older stars.

The angular momentum loss by the solar mass stars in the considered range of ages is not very significant (Stauffer & Soderblom 1991). The dependence of Fig. 7 was simulated assuming the angular momentum to be conserved. The initial rotation period for the age of 1.9 Myr was assumed equal to 5 days. The period decreased to less than 1 day over the 30 Myr due to the decrease in the momentum of inertia of the contracting star. A subsequent increase of the period to the present day solar value should be mainly attributed to the early main-sequence evolution (Stauffer & Soderblom 1991; Endal & Sofia 1981). Table 2

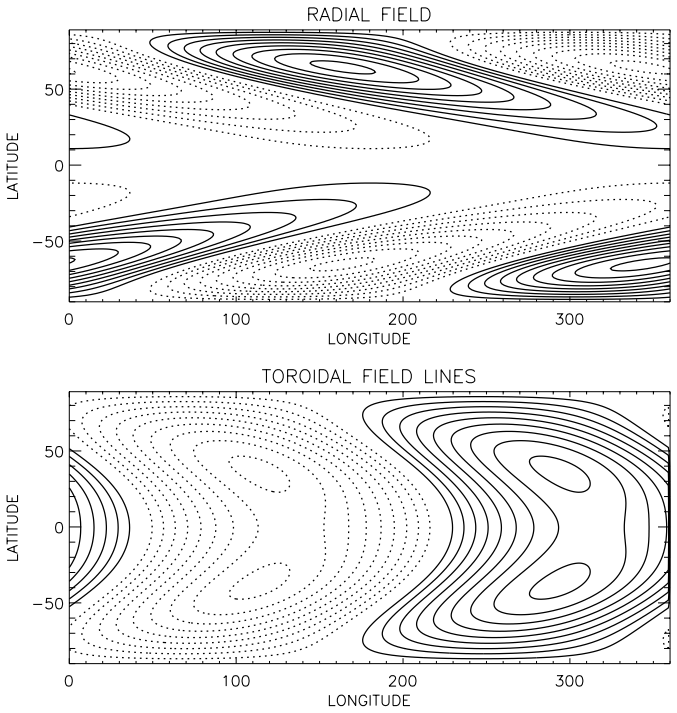

Fig. 5. Isolines of the radial field and the toroidal field lines for the marginal A1-mode on the spherical surface of $r = R/2$. Full lines show positive levels and clockwise circulation and vice versa for the dashed lines. $P_{\rm rot} = 5$ day.

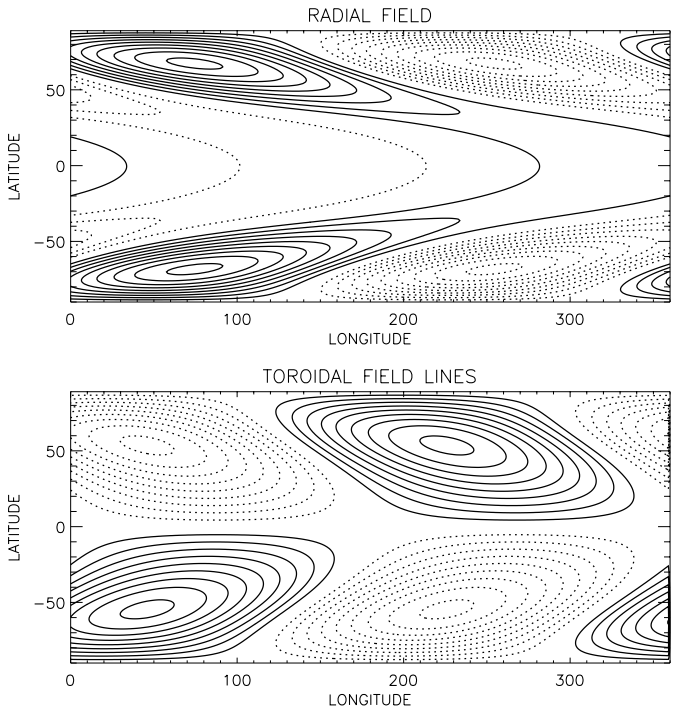

Fig. 6. The same as in Fig. 5 but for the marginal S1 mode.

lists the rotation periods for the ages for which the dynamo simulations were performed.

The same Table also shows the values of the C_Ω-parameter (14). The increase of C_Ω with age indicates the increased role of differential rotation. This is,

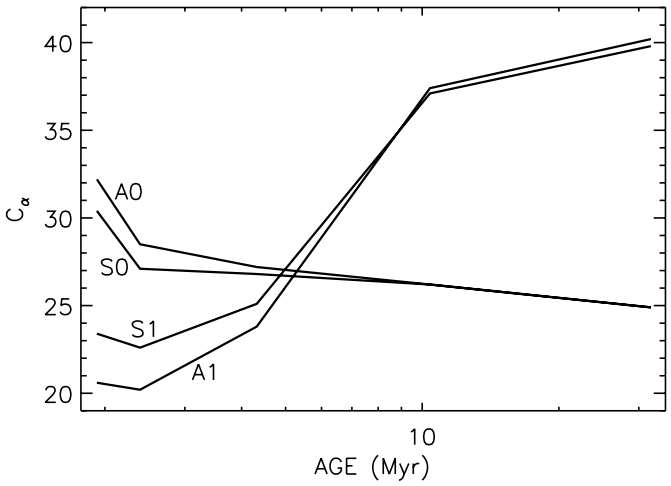

Fig. 7. The dependence on the stellar age of the threshold dynamo numbers for different symmetry types of the dynamo-generated fields.

Table 2. Rotation periods and C_Ω values for several ages of the core growth epoch.

Age (Myr)	1.92	2.39	4.32	10.4	31.9
$P_{\rm rot}$ (day)	5.00	4.36	3.03	1.77	0.68
C_Ω	240	250	280	507	2180

probably, the main reason for the change from nonaxisymmetry to axisymmetry in the global magnetic field. The differential rotation favors axisymmetry (Rädler 1975; Rüdiger & Elstner 1994; Moss & Brandenburg 1996), as discussed above. The increase of C_Ω is mainly due to the rotational quenching of the eddy diffusivity. Equation (7) describes the decrease of η (6) in inverse proportion to the rotation rate, $\eta = \eta_{\rm T} 3\pi/(8\Omega^*)$, for the rapid rotation case, $\Omega^* \gg 1$. E.g., the largely inhomogeneous profiles of $\eta_{\rm T}$ and Ω^* of Fig. 3 result in an almost uniform diffusivity $\eta \simeq 3 \times 10^{12}$ cm^2 s^{-1} due to the quenching effect. An account of the angular momentum loss by the star would shift the change in the axial symmetry in Fig. 7 to a somewhat older age.

3.3. Internal field capture

The magnetic flux capture by the growing core was treated with a largely simplified model. The model neglects the stellar radius dependence on time and assumes rigid rotation but keeps the essential anisotropy of the α-effect. The model should be nonlinear in order to estimate the amplitude of the internal field. We used the simplest nonlinearity of the so-called global quenching of the α-effect to this end.

$$\alpha_{ij} = C_\alpha \frac{\eta_{\rm t} r}{R^2(1+ < B^2 >_{cz} / B_0^2)} \, (\delta_{ij} - e_i e_j) \cos\theta. \qquad (20)$$

In this equation, B_0 is the convective energy equipartition field and the angular brackets signify the averaging over volume of the convection zone. The global quenching allows the azimuthal wave number to be fixed so that the nonlinear dynamics of a 3D nonaxisymmetric field can be simulated by solving 2D equations.

The anisotropy of the magnetic field diffusivity is neglected. The total diffusivity, $\eta = \eta_c + \eta_t$, combines the microscopic, η_c, and turbulent, η_t, constituents. η_c is assumed constant everywhere and η_t is constant in the proper convection zone but falls to zero in a thin (overshoot) layer of thickness d centered around the core radius, x_c. The diffusivity profile in the transition layer is approximated by the cubic spline,

$$\eta_t = \begin{cases} 0 & \text{for } x \le x_c - d/2 \\ \frac{\eta_0}{2}(1 + \frac{x-x_c}{d^3}(3d^2 & \text{for } |x - x_c| \le d/2 \\ \quad -4(x-x_c)^2)) & \\ \eta_0 & \text{for } x \ge x_c + d/2 \end{cases} . \quad (21)$$

The time-dependence of the core radius was approximated by the power law, $x_c \sim (t - t_c)^{1/4}$, shown by the dotted line in Fig. 1.

The induction Eq. (2) was solved numerically in the whole sphere by time-stepping, starting from an initial weak magnetic field. The input parameters for the model are the C_α, the fractional thickness, d, of the overshoot layer, the convection zone-to-core diffusivity ratio, η_0/η_c, the diffusive time, $T_d = R^2/\eta_0$, and the equipartition field, B_0. Figure 8 illustrates the results of the run made with about five times supercritical $C_\alpha = 100$, the transition layer thickness $d = 0.1$, and the other parameter values inferred from the stellar structure model: $\eta_0/\eta_c = 10^7$, $T_d = 250$ yrs, and $B_0 = 2000$ G.

The plots show the results for the preferentially excited nonaxisymmetric fields of $m = 1$. The runs are rather expensive in computation time because of the large difference between the diffusive and evolutionary times. The computations were terminated at the age of 5 Myr where Fig. 7 indicates the change in the axial symmetry. We considered both types of equatorial symmetry because the preference we have found for the A1-mode may not be very reliable. The threshold dynamo numbers of Fig. 4 for the S1 and A1 modes are quite close. The discrimination between the two equatorial symmetry types is a matter of the details of the rotation law. Küker & Rüdiger (1999) found S1 as the dominating mode for a fully convective, rigidly rotating star. There is no contradiction with our model, however, because we also find the S1-mode to have the smallest threshold dynamo number when neglecting the differential rotation. Anyway, the two panels of Fig. 8 show similar results.

Initially, the field is amplified to several kilogauss in about a diffusive time and its amplitude remains almost steady afterwards. There is no internal field at the beginning of the run because the core has not formed yet. The

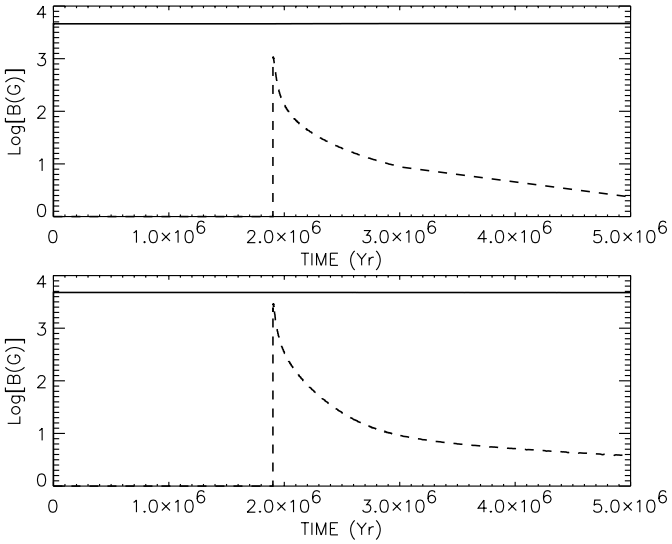

Fig. 8. The volume-averaged rms magnetic fields of convection zone (full line) and radiative core (dashed) as functions of stellar age. The top and bottom panels show the results for the A1 and S1 symmetry types respectively.

core formation manifests itself by a sharp peak in the internal field. Fields of kilogauss strength are captured initially. The volume-averaged rms internal field decreases, however, with time and falls to the amplitude of several Gauss at the end of the run when the core grows to about 35% in radius. The field strength in the convection zone meanwhile remains almost unchanged. The internal field should be comparable in strength to the dynamo-field in order to influence the dynamo operation (Moss 1996), which is not the case with our model.

The reason why the field cannot be captured efficiently is its nonstationary nature. The amplitude of the field in the convection zone is almost constant. The field structure is not steady, however. The nonaxisymmetric field pattern drifts in azimuth, completing one revolution in the co-rotating reference frame in about a diffusive time. Therefore, a given angular position on the surface of the growing core is "seeing" a field oscillating with a pattern drift period. The oscillatory field is most efficiently captured at the initial stages of most rapid core growth. This explains why the internal field for the A1 mode is smaller compared to S1: the magnetic field in the center of the star is zero for A1 but finite for S1. We find that almost no new (poloidal) flux is captured at the final stages of the runs. Only the field which is already rooted in the radiative interior is joined to the core at those stages.

The efficiency of the field capturing would increase if the local dynamo-number in the overshoot region were larger than in the convection zone proper (Parker 1981). The above expressions (10), (19) for the α-effect do not support such a case, however.

Extrapolating the dependencies of Fig. 8, we expect that the rms internal field is somewhat below 1 G when the core grows to the present-day solar value of $x_c \simeq 0.7$. The field suffices, however, to link the core rotation to

the convective envelope (Charbonneau & McGregor 1993; Rüdiger & Kitchatinov 1996). It is also strong enough to ensure the change from differential to rigid rotation in the solar tachocline (Kitchatinov & Rüdiger 1996; McGregor & Charbonneau 1999). The nonaxisymmetry of the internal field changes the tachocline problem qualitatively, however. Mestel & Weiss (1987) and Moss (1992) noted that Maxwell stress from a nonaxisymmetric field is very efficient at reducing differential rotation. Moreover, the interaction of a nonuniform rotation with the internal field should excite a nonaxisymmetric flow (global vortices) via the nonaxisymmetric Lorentz force. Then, the angular momentum will be transported not by Maxwell stress alone, as in the axisymmetric case, but by Reynolds stress as well.

The nonaxisymmetry of the internal field predicted by our model may be relevant to the active longitudes observed in solar and stellar activity. Berdyugina & Tuominen (1998) and Korhonen et al. (1999) reported observations of the "flip-flop" phenomenon in stellar magnetic cycles. One active longitude prevails over a given half-cycle. The longitudinal position of the enhanced activity region is changed by 180° over the next half-cycle but returns to the original position after a complete magnetic cycle. The phenomenon can be interpreted, at least qualitatively, in terms of the internal magnetic field. The nonaxisymmetric relic field is rooted in a rigidly rotating core but penetrates the convective shell where differential rotation pulls an azimuthal steady field from it. A superposition of the nonaxisymmetric azimuthal field of internal origin with the toroidal field of the axisymmetric dynamo makes an enhanced field on the longitude region where both fields coincide in sign. After a half of the activity cycle, the dynamo-field reverses and the enhanced field position jumps by 180° over longitude. It returns to the original position after a complete magnetic cycle.

The longitudes of enhanced activity were also inferred from the statistics of solar active regions (Vitiskij 1969, 1982; Benevolenskaya et al. 1999) and solar flares (Jetsu et al. 1997). The very notion of a fixed (active) longitude implies a rigid rotation. The homogeneous rotation can be found only in the radiative core of the Sun (Shou et al. 1998). The nonaxisymmetric relic field rooted in the core may be the reason why the solar activity statistics lack axial symmetry.

The alternative possibility should be mentioned, however, that a nonlinear dynamo alone can support deviations from axial symmetry in the global magnetic field. Moss (1999) show that stable mixed axial symmetry solutions can exist in a certain parameter range of a solar-type dynamo.

As a prospective for extension of the present theory, nonaxisymmetric magnetic fields of A-stars can be noticed. Recently Stepień (2000) suggested that the effect of the pre-main sequence field in A-stars may be crucial in determining their subsequent rotation rates. The more massive stars evolve faster. A more rapid growth of radiative zones in A-stars should lead to stronger "relic" fields compared to that predicted for the Sun. It is currently not clear, however, whether the kilogauss nonaxisymmetric fields of Ap-stars can be explained in this way (cf. Moss 1989).

Acknowledgements. MMJ was funded by a PPARC Advanced Fellowship. LLK was funded by PPARC grant GR/L00827. This work was supported in part by the Russian Foundation for Basic Research (Project 99-02-16088).

References

Basri, G., Marcy, G. W., & Valenti, J. A. 1992, ApJ, 390, 622
Benevolenskaya, E. E., Hoeksema, J. T., Kosovichev, A. G., & Scherer, P. H. 1999, ApJ, 517, 163
Berdyugina, S. V., & Tuominen, I. 1998, A&A, 336, 25
Brandenburg, A., Krause, F., Meinel, R., Moss, D., & Tuominen, I. 1989, A&A, 213, 411
Cattaneo, F., & Vainshtein, S. I. 1991, ApJ, 376, L21
Chandrasekhar, S. 1961, Hydrodynamic and hydromagnetic stability (Clarendon Press, Oxford), 622
Charbonneau, P., & McGregor, K. B. 1992, ApJ, 343, 526
Charbonneau, P., & McGregor, K. B. 1993, ApJ, 417, 762
Donati, J.-F., & Cameron, A. C. 1997, MNRAS, 291, 1
Dudorov, A. E., Krivodubskij, V. N., Ruzmaikina, T. V., & Ruzmaikin, A. A. 1989, SvA, 33, 420
Durney, B. R. 1989, ApJ, 338, 509
Eggleton, P. P. 1971, MNRAS, 151, 351
Eggleton, P. P. 1972, MNRAS, 156, 361
Eggleton, P. P. 1973, A&A, 23, 325
Endal, A. S., & Sofia, S. 1981, ApJ, 243, 625
Gilliland, R. L. 1986, ApJ, 300, 339
Hartmann, L. W., & Noyes, R. W. 1987, ARA&A, 25, 271
Jetsu, L., Pohjolainen, S., Pelt, J., & Tuominen, I. 1997, A&A, 318, 293
Kitchatinov, L. L., & Rüdiger, G. 1996, AstL, 22, 279
Kitchatinov, L. L., & Rüdiger, G. 1999, A&A, 344, 911
Kitchatinov, L. L., Pipin, V. V., & Rüdiger, G. 1994, Astron. Nachr., 315, 157
Korhonen, H., Berdyugina, S. V., Hackman, T., et al. 1999, A&A, 346, 101
Krause, F., & Meinel, R. 1988, Geophys. Astrophys. Fluid Dyn., 43, 95
Krause, F., & Rädler, K.-H. 1980, Mean–Field Magnetohydrodynamics and Dynamo Theory (Akademieverlag, Berlin)
Küker, M., & Rüdiger, G. 1997, A&A, 328, 253
Küker, M., & Rüdiger, G. 1999, A&A, 346, 922
McGregor, K. B., & Charbonneau, P. 1999, ApJ, 519, 911
Mestel, L. 1965, QJRAS, 6, 265
Mestel, L., & Weiss, N. O. 1987, MNRAS, 226, 123
Moss, D. 1989, MNRAS, 236, 629
Moss, D. 1992, MNRAS, 257, 593
Moss, D. 1996, A&A, 305, 140
Moss, D. 1999, MNRAS, 306, 300
Moss, D., & Brandenburg, A. 1996, Geophys. Astrophys. Fluid Dyn., 80, 229
Moss, D., Tuominen, I., & Brandenburg, A. 1991, A&A, 245, 129
Moss, D., Barker, D. M., Brandenburg, A., & Tuominen, I. 1995, A&A, 294, 155

Nordlund, Å., Galsgaard, K., & Stein, R. F. 1994, Magnetoconvection and magnetoturbulence, in Solar Surface Magnetic Fields, ed. R. J. Rutten, & C. J. Schrijver, NATO ASI Ser., vol. 433, 471
Parker, E. N. 1955, ApJ, 122, 293
Parker, E. N. 1979, Cosmical magnetic fields (Clarendon Press, Oxford)
Parker, E. N. 1981, Geophys. Astrophys. Fluid Dyn., 18, 175
Pudovkin, M. I., & Benevolenskaya, E. E. 1984, SvA, 28, 458
Rädler, K.-H. 1975, Mem. Soc. Sci. Liège, 6 Ser., 8, 109
Rädler, K.-H., Wiedemann, E., Brandenburg, A., Meinel, R., & Tuominen, I. 1990, A&A, 239, 413
Rogers, F. J., & Iglesias, C. A. 1992, ApJS, 79, 507
Rüdiger, G., & Elstner, D. 1994, A&A, 281, 46
Rüdiger, G., & Kitchatinov, L. L. 1993, A&A, 269, 581
Rüdiger, G., & Kitchatinov, L. L. 1996, ApJ, 466, 1078
Schou, J., Antia, H. M., Basu, S., et al. 1998, ApJ, 509, 456
Schüssler, M. 1975, A&A, 38, 263
Spruit, H. 1987, Angular momentum transport in the radiative interior of the sun, in The Internal Solar Angular Velocity, ed. B. Durney B., & S. Sofia (D. Reidel, Dordrecht), 185
Stauffer, J. R., & Soderblom, D. R. 1991, The evolution of angular momentum in solar mass stars, in The Sun in Time, ed. C. P. Sonett, M. S. Giampapa, & M. S. Matthews (Univ. Arizona Press, Tucson), 832
Stepień, K. 2000, A&A, 353, 227
Tayler, R. J. 1987, MNRAS, 227, 553
Vitinskij, Yu. I. 1969, Solar Phys., 7, 210
Vitinskij, Yu. I. 1982, Soln. Dannye, 2, 113
Weiss, A., Keady, J. J., & Magee, N. H. 1980, At. Data Nucl. Data Tables, 45, 209